Organic Process Research & Development **2006**, *10,* 717−722

Seeding and Constant-Supersaturation Control by ATR-FTIR in Anti-Solvent Crystallization

Zai Qun Yu,*,† Pui Shan Chow,‡ and Reginald B. H. Tan†,‡

Department of Chemical & Biomolecular Engineering, National University of Singapore, 10 Kent Ridge Crescent, Singapore 119260, and Institute of Chemical and Engineering Sciences Ltd., 1 Pesek Road, Jurong Island, Singapore 627833

Abstract:

The strategy for seeding and supersaturation control can play a critical role in defining the purity and particle size distribution of crystal products. Previous research has demonstrated that operation of crystallizers at constant supersaturation by feedback control is attractive due to its simplicity and resistance to operating disturbances. In this study, the effects of seed loading and seed size distribution were investigated for anti-solvent crystallization of paracetamol from a water−acetone mixture operated at constant supersaturation. A seeding strategy based on a simple mass balance equation provided a good starting point for the refinement of particle size distribution and adjustment of batch time in different circumstances to obtain a target average crystal size with narrow size distribution.

Introduction

Seeding and supersaturation profile have been identified as two critical factors in batch crystallization control in order to consistently produce high-purity crystals with narrow particle size distribution (PSD) and large average size.[1] The uncertainties in stochastic primary nucleation occurring in unseeded crystallization, which contributes much to the variations in crystal number and particle size from batch to batch, are circumvented by seeding. Manipulation of supersaturation profile, on the other hand, avoids fast crystal growth which is responsible for mother liquor inclusion and excessive secondary nucleation which generates nuclei with various lifetimes and thus widens the final PSD.

Varying attention has been paid to these two aspects by different researchers. Research on seeding technique has been mainly targeted towards how to determine seed size and seed loading. Kubota et al.[2] emphasized the importance of seed loading to guarantee the unimodal distribution of final products. Their work showed that unimodal distribution of final products could be achieved with a wide range of generation rates of supersaturation when seed loading exceeded a critical value which was determined empirically. One consequence of accommodating high generation rates of supersaturation is the high seed loading which inevitably compromises productivity. Lung-Somarriba et al.[3] put forward a procedure to determine seed size and seed loading which took into consideration the attrition of large crystals. They proposed that the seed size should be smaller than one-quarter of the maximal product size over which attrition will hinder crystal growth. Similar to the critical seed loading proposed by Kubota et al.,[2] they used critical surface area obtained empirically to determine the size-mass couple of seeds. Guwald and Mersmann[4] incorporated generation rate of supersaturation in the calculation of seed loading. For a given cooling crystallization system with a cooling rate of $\dot{T}$, the necessary seed mass M_S was:

$$M_S = -\frac{\varphi_v}{\varphi_a}\left(\frac{dc^*}{dT}\right)M_{sol}\frac{\dot{T}\bar{L}_S}{G_{met}}\left(1+\frac{1}{2}\frac{G_{met}\Delta T_{met}}{\dot{T}L_S}\right)^2 \qquad (1)$$

where φ_v and φ_a are the volume and surface shape factors of crystals respectively, $\bar{L}_S$ is the average seed size, dc^*/dT is the slope of the solubility curve, M_{sol} is the mass of solvent, G_{met} is the maximum allowable growth rate within the metastable zone, and ΔT_{met} is the maximum allowable undercooling. It can be seen that this seeding policy integrates important operating parameters, two of which need to be measured separately, namely G_{met} and ΔT_{met}.

Previous work on supersaturation control has been based on process modeling with varying degrees of complexity in which crystallization kinetics must be known. The key issue in the choice of supersaturation profile is that it must strike a balance between nucleation suppression and acceptable operating time: low enough to suppress secondary nucleation but high enough to complete one batch in a reasonable time frame. Excessive nucleation and fast crystal growth under high supersaturation are usually accompanied by a large uptake of impurities. A typical strategy in early studies on cooling crystallization was to maintain a reasonably low constant supersaturation level throughout operation, as in the groundbreaking work by Mullin and Nỳvlt [5] where the temperature of crystallizers followed the so-called "programmed cooling" profile, leading to a significant increase in average crystal size. Of course the supersaturation is not necessarily constant, but it should be kept within the metastable zone to suppress secondary nucleation.[6] On the other hand, keeping it constant simplifies the deduction of operating lines to some degree. For instance, under a few strong assumptions, Mullin pointed out that the temperature profile for general application should be cubic in time in seeded

* To whom correspondence should be addressed. Telephone: +65-67963844. Fax: +65-63166183. E-mail: g0203703@nus.edu.sg.

† National University of Singapore.

‡ Institute of Chemical and Engineering Sciences Ltd.

(1) Paul, E. L.; Tung, H. H.; Midler, M. *Powder Technol.* **2005**, *150*, 133−143.

(2) Kubota, N.; Doki, N.; Yokota, M.; Sato, A. *Powder Technol.* **2001**, *121*, 31−38.

(3) Lung-Somarriba, B. L. Moscosa-Santillan, M.; Porte, C.; Delacroix, A. *J. Cryst. Growth* **2004**, *270*, 624−632.

(4) Mersmann, A. *Crystallization Technology Handbook*, 2nd ed.; Marcel Dekker: New York, 2001; p 410.

(5) Mullin, J. W.; Nỳvlt, J. *Chem. Eng. Sci.* **1971**, *26*, 369−377.

(6) Jones, A. G.; Mullin, J. W. *Chem. Eng. Sci.* **1974**, *29*, 105−118

10.1021/op060058j CCC: $33.50
Published on Web 05/09/2006

crystallization to maintain a constant supersaturation:[7]

$$T = T_I - (T_I - T_F)\left(\frac{t}{\tau}\right)^3 \quad (2)$$

where τ is the overall batch time and t is any time during the process. T_I and T_F denote the initial and final slurry temperature, respectively.

Combination of seeding technique and manipulation of supersaturation profile increases the likelihood of removing inconsistency from final PSD. Mullin[7] proposed an expression based on McCabe's ΔL law[8] to determine the seed mass-size couple which has the following equivalent form:

$$\left(\frac{\bar{L}_S}{\bar{L}_P}\right)^3 = \frac{M_S}{M_P} \quad (3)$$

where $\bar{L}_P$ and M_P stand for the final average product size and mass (the product mass consists of two parts: seed mass and the mass of solute that has deposited on seed surfaces). This expression is derived from a mass balance of the crystallization batch by assuming the number of product crystals to be equal to that of seeds. It should be noted that $\bar{L}_S$ and $\bar{L}_P$ are number-mean size, defined as the first moment of the normalized population density function. In conjunction with programmed cooling, it is assumed that nucleation is subdued to such a degree that almost all solute molecules deposit on the seed surfaces, and the product size is then related to seed mass-size couple by eq 3. Genck[9] presented two examples on the application of this methodology to cooling and evaporative crystallizations.

The concept of "optimal control"[10] of crystallization takes a step further beyond the above-mentioned "programmed cooling" in that the control objective is now to obtain the best properties of final products such as maximum average size, minimum coefficient of variation (*CV*), minimum mass ratio of newly formed crystals to grown seeds, shortest batch time or combination of them, etc. by manipulating temperature trajectory, whereas the explicit control goal of programmed cooling is just to maintain supersaturation at a certain level. Optimization is employed to derive the optimal temperature profile which depends heavily on the objective function. For example, minimization of *CV* in unseeded crystallization leads to fast cooling at the beginning of the operation with the goal to generate nuclei in a short time interval, while maximization of average size necessitates the convex temperature profiles. Jones[10] found that the supersaturation profile to maximize the terminal size of seeds departs remarkably from a straight line.

Instead of treating seeding policy separately from supersaturation profile, Chung et al.,[11] and Choong and Smith[12] included seed properties as the optimized variables along with temperature profile in the formulation of optimization problems. The relationship between the properties of seeds and products is complicated by secondary nucleation whose rate is usually a function of the third moment and/or average size of the particles in the slurry. Growth rate dispersion and agglomeration lead to further complication and all of them can be accounted for in the models.[13,14] It is noteworthy that any form of nucleation and agglomeration are neglected in eq 3, resulting in exactly the same distribution of products as that for the seeds except for the average size in an ideal situation.

Traditionally, the model-based strategies reviewed above have been implemented by open-loop control in which a temperature profile corresponding to constant supersaturation or optimal control is tracked by a temperature controller of PID type as a series of set-points. The crystallization performance is contingent on model complexity, the uncertainties in parameter estimation, and operating disturbance. Simplified models may fail to capture the process dynamics satisfactorily, causing the optimal trajectory deduced from optimization to go astray. Uncertainties in parameter estimation are inherent and related to the random errors in experimental data. Operating disturbances are inevitable since crystallizers are located downstream to various synthesis trains. The actual supersaturation, therefore, may be far from its theoretical values in open-loop control strategies. Efforts have been made to handle these issues via model improvement and robust control theory.[15] At the same time, the drawbacks in open-loop control listed above can be circumvented by closed-loop control of supersaturation.[16−21] At every sampling instant, the actual transient supersaturation is calculated from the solubility curve and the measured solute concentration and compared with its set point; then the target crystallizer temperature, to make them equal, is calculated and fed back to the temperature controller as the temperature set point for the next interval. Obviously supersaturation control possesses the capability to absorb some disturbances in operating conditions, such as changes in initial solute concentration, seed loading, and crystal growth rate, etc.

With supersaturation control ready at hand, one may ask which is preferred for the set-point profile of supersaturation: a constant value or a robust optimal trajectory deduced from optimization? Theoretically the latter choice is better when it makes a big difference from the former operation as demonstrated by Jones.[10] However, the former choice is also attractive due to its simplicity for commercial application: no kinetics study, no process models, no optimization, and no concerns about parameter uncertainties. After all, it

(7) Mullin, J. W. *Crystallization*, 4th ed.; Butterworth-Heinemann: Oxford, 2001; p 393.
(8) McCabe, W. L. *Ind. Eng. Chem.* **1929**, *21*, 112−119.
(9) Genck, W. *J. Chem. Eng. (New York)* **2000**, *107*, 90−95.
(10) Jones, A. G. *Chem. Eng. Sci.* **1974**, *29*, 1075−1087
(11) Chung, S. H.; Ma, D. L.; Braatz, R. D. *Can. J. Chem. Eng.* **1999**, *77*, 590−595.
(12) Choong, K. L.; Smith, R. *Chem. Eng. Sci.* **2004**, *59*, 313−327.
(13) Hu, Q.; Rohani, S.; Wang, D. X.; Jutan, A. *Powder Technol.* **2005**, *156*, 170−176.
(14) Costa, C. B. B.; da Costa, A. C.; Filho, R. M. *Chem. Eng. Process.* **2005**, *44*, 737−753.
(15) Nagy, Z. K.; Braatz, R. D. *J. Process Control* **2004**, *14*, 411−422.
(16) Jones, A. G.; Teodossiev, N, M. *Cryst. Res. Technol.* **1988**, *23*, 957−966.
(17) Liotta, V.; Sabesan, V. *Org. Process Res. Dev.* **2004**, *8*, 488−494.
(18) Feng, L. L.; Berglund, K. S. *Cryst. Growth Des.* **2002**, *2*, 449−452.
(19) Grön, H.; Borissova, A. K.; Roberts, J. *Ind. Eng. Chem. Res.* **2003**, *42*, 198−206.
(20) Yu, Z. Q.; Chow, P. S.; Tan, R. B. H. *Ind. Eng. Chem. Res.* **2006**, *45*, 438−444.
(21) Fujiwara, M.; Nagy, Z. K.; Chew, J. W.; Braatz, R. D. *J. Process Contr.* **2005**, *15*, 493−504.

performs similarly as the latter in some cases. Worlitschek and Mazzotti[22] showed that optimized cooling led to a volume-weighted PSD of paracetamol rather close to that of a constant supersaturation (in terms of concentration difference). Moreover, implementation of constant supersaturation via feedback control facilitates the development of crystallization processes in that it offers a quick assessment of batch time and product quality at different supersaturation levels. As the critical factor in crystallization protocols, the set point of supersaturation can be determined readily from a small number of batches along with other operating parameters aided by design of experiment (DOE).

This paper presents results of the first attempt to explore an optimal seeding policy at constant supersaturation without resorting to optimization in anti-solvent crystallization. Basically the calculation of seed size-mass couple is based on eq 3 as used by Mullin[7] and Genck,[9] and feedback control of supersaturation is implemented via attenuated total reflection-Fourier-transform IR spectroscopy (ATR-FTIR) technique. In anti-solvent crystallization of paracetamol from a water−acetone mixture, the effects of different seed size are evaluated and followed by the effects of seed loading and seed size distribution. In a previous study conducted by the same authors,[20] it was reported that seeded crystallization yielded a much better PSD than unseeded crystallization. However, only milled seeds were applied in that case and seeding policy was not investigated in detail. This paper will focus on how to minimize secondary nucleation by careful seeding. The relationship between secondary nucleation and agitation intensity (contingent on particular properties of model system, e.g. hardness of crystals, crystal yield and productivity) are not considered herein, but it can be readily incorporated into the framework used in this study through additional experiments.

Experimental Section

1. Materials and Instrumentation. Paracetamol powder supplied by Sigma Chemical Co., pro-analysis grade acetone provided by Merck (≥99.5%) and deionized water were used to prepare the solutions.

Calibration of ATR-FTIR and the structure of supersaturation control have been described previously.[20] Absorbance spectra were collected with a resolution of 4 cm^{-1} on a Nicolet 4700 spectrophotometer (Nicolet Instrument Co.) equipped with a Dipper-210 ATR-FTIR immersion probe (Axiom Analytical Inc.). Every spectrum was the average of 64 scans in the range of 600 to 4000 cm^{-1}. Spectra of deionized water at 23 °C were used as background. The FTIR machine was purged continuously by purge gas supplied by a FTIR purge gas generator (model 75−52−12VDC, Parker Balston).

A FBRM probe (Model D600L, Lasentec) was inserted into the turbulent zone of the suspension. Its prominent advantage of in-situ measurement removes the errors incurred during off-line sampling and provides continuous information on the solid phase during the crystallization process. FBRM data were displayed and analyzed in the Control Interface software version 12 which provides chord length distribution (CLD) and related statistics.

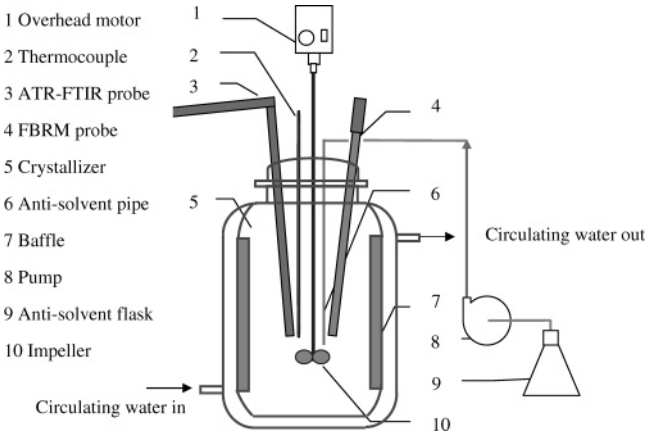

Figure 1. **Experimental setup for anti-solvent crystallization.**

Normalized population density of final products was obtained by sieve analysis (Sonic sifter, model L3P from ATM Co.). All particles retained on one sieve were assumed to have the same size L_i, i.e., the arithmetic mean aperture size of two adjacent sieves. The mass of crystals retained on every sieve, M_i, was converted to the number of particles, N_i, according to eq 4:

$$M_i = N_i \rho \varphi_v L_i^3 \tag{4}$$

where $\rho = 1293$ kg/m^3, $\varphi_v = 0.6465$ ($\varphi_v$was obtained by the method described by Mullin:[7] weighing the mass of a known number of crystals sampled from a sieve fraction, then calculating φ_v according to eq 4). Average particle size $\bar{L}$, standard deviation σ, and CV from sieve analysis are calculated as:

$$\bar{L} = \frac{\sum N_i L_i}{\sum N_i} \tag{5}$$

$$\sigma^2 = \frac{\sum (L_i - \bar{L})^2 N_i}{\sum N_i} \tag{6}$$

$$CV = \frac{\sigma}{\bar{L}} \tag{7}$$

The *CV* of PSD was used as a measure of size distribution spread.

2. Experimental Procedures. The experimental setup for anti-solvent crystallization studies is shown schematically in Figure 1. The main vessel was a 1-L flat-bottomed glass crystallizer with an inner diameter of 100 mm. It was fitted with four glass baffles on the inner wall. A marine-type impeller made of stainless steel with a diameter of 42 mm rotating at 500 rpm was used to provide agitation. The gap between the impeller and the crystallizer bottom was 43 mm, about one-third of the final working height of the suspension. A computerized peristaltic pump (MasterFlex 7550) was connected to the control system to maintain the relative supersaturation at 0.05, and its maximum flow rate was set at 5 g/min. To suppress nucleation and sustain a moderate crystal growth 0.05 was found to be a proper supersatura-

(22) Worlitschek, J.; Mazzotti, M. *Cryst. Growth Des.* **2004**, *5*, 891−903.

Table 1. **Experimental conditions, PSD statistics of products and curve-fitting for profiles of accumulated anti-solvent mass**

no.	seed fraction, μm	target product size, μm	actual product size, μm	*CV* of products, %	curve-fitting for profiles of accumulated anti-solvent mass
1	250−300	600	395	65.96	$20.34 + 2.56t - 0.044t^2 + 0.0006t^3$, $R^2 = 1.0000$
2	212−250	600	431	53.22	$30.79 + 1.02t - 0.0093t^2 + 0.0002t^3$, $R^2 = 0.9996$
3	150−180	600	472	46.86	$26.35 + 1.35t - 0.021t^2 + 0.0002t^3$, $R^2 = 0.9984$
4	212−250	476	514	23.67	$46.49 + 1.35t - 0.0098t^2 + 0.0004t^3$, $R^2 = 0.9997$
5	150−180	476	496	25.89	$23.74 + 0.93t - 0.011t^2 + 0.0001t^3$, $R^2 = 0.9985$
6	<125	476	509	36.32	$32.28 + 0.75t - 0.010t^2 + 0.00007t^3$, $R^2 = 0.9971$

tion.[20] The injection point was 5 mm above the impeller tip to accelerate dispersion.

Initial solutions were prepared in such a way that they were slightly supersaturated when cooled to 23 °C. Paracetamol (108.2 g) was dissolved in 400 g of water−acetone mixture with ∼45 wt % of acetone. Then the temperature was elevated to 45 °C and maintained for 30 min to ensure all paracetamol crystals have dissolved. After that the temperature was lowered to 23 °C and allowed to stabilize for 10 min before the addition of seeds and anti-solvent. Water (500 g) was pumped into the crystallizer in total, and agitation speed was fixed at 500 rpm for all runs. It has been shown that, under our present experimental conditions, a stirring speed of 500 rpm was sufficient for effective dispersion of anti-solvent and for lessening localized nucleation near the injection point.[23] The final acetone concentration was ∼20 wt %. At the completion of every run, crystal products were isolated by vacuum filtration of the slurry followed by ambient drying.

Seeds of various sizes were prepared by sieving the products harvested from unseeded crystallization in the same crystallizers. Seeds were applied without washing. Paracetamol crystals tend to agglomerate in acetone−water mixtures,[24] so the seeds were actually a mixture of well-formed crystals and agglomerates. Growth on the rough surfaces of seeds will inevitably lead to irregular appearance of products and decreasing values of volume shape factor, φ_v, distorting the relationship reflected in eq 3 wherein products and seeds are assumed to have the same value of φ_v.

Results and Discussion

Six runs of experiment were carried out in total, as summarized in Table 1. In all experiments, the mass of solute to be deposited on seed surfaces is calculated to be ∼41.5 g (i.e., $M_P - M_S$), based on a theoretical yield of 38.35%. Then eq 3 can be rewritten as:

$$\left(\frac{\bar{L}_S}{\bar{L}_P}\right)^3 = \frac{M_S}{41.5 + M_S} \tag{8}$$

It can be seen that M_S increases with $\bar{L}_S$ when $\bar{L}_P$ is fixed. A larger product size means less total surface area for the adsorption of impurity molecules and less resistance of filtration cakes, which is the reason it has been chosen as a frequent objective of crystallization studies. In production practice the desired crystal size is contingent on circumstances: for example, an intermediate crystal size range may be preferable for quick dissolution in subsequent processing.[17]

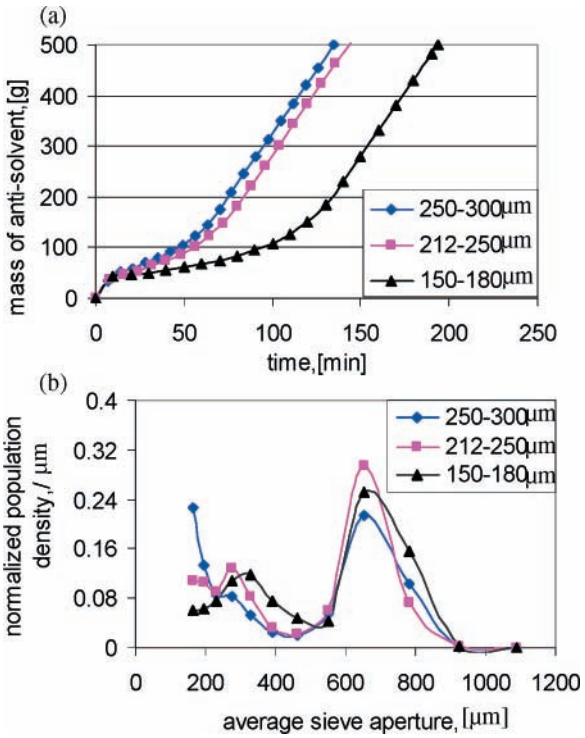

Figure 2. **Results of seeded crystallization with different seed sizes. (a) Trajectories of anti-solvent mass. (b) PSD of products.**

1. Effects of Seed Size. Seeds of three different size fractions obtained by sieving were used in this initial investigation (runs 1−3 in Table 1): 250−300 μm ($\bar{L}_S$ = 275 μm, M_S = 4.41 g), 212−250 μm ($\bar{L}_S$ = 231 μm, M_S = 2.51 g), and 150−180 μm ($\bar{L}_S$ = 165 μm, M_S = 0.88 g). The desired product size, $\bar{L}_P$, was specified to be 600 μm. The seed mass-size couples were obtained according to eq 3. The resulting trajectories of accumulated mass of anti-solvent and the PSD of products are shown in Figure 2.

From Figure 2a it can be seen that the batch time varies with seed mass-size couples. The batch time with $\bar{L}_S$ = 165 μm was 194 min, while the batch time with $\bar{L}_S$ = 275 μm was only 135 min. The batch with larger seeds has a larger total surface area for crystal growth: therefore, the batch time was shortened accordingly. The bimodal distributions in Figure 2b indicate that significant secondary nucleation occurred in the three runs.

An inspection of the features in Figure 2 reveals two trends. First, a distinct and prominent peak occurs at around

(23) Yu, Z. Q.; Tan, R. B. H.; Chow. P. S. *J. Cryst. Growth* **2005**, *279*, 477−488.
(24) Uusi-Penttila, M. S.; Rasmuson, A. C. *Trans. Inst. Chem. Eng.* **2003**, *81*, Part A, 489−495.

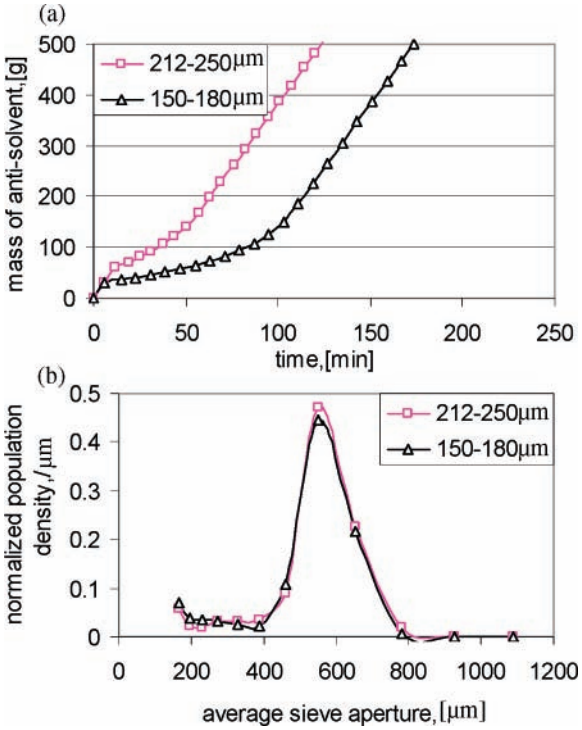

Figure 3. **Results of seeded crystallization with doubled seed loadings. (a) Trajectories of anti-solvent mass. (b) PSD of products.**

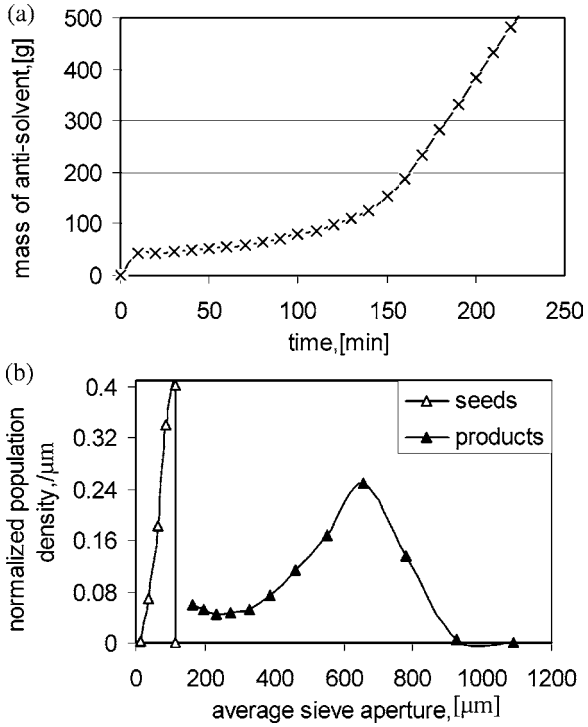

Figure 4. **(a) Trajectories of anti-solvent mass and (b) PSD of seeds smaller than 125 μm and resulting crystal products**

650 μm (slightly larger than the expected product size, 600 μm), indicating the feasibility of the seeding methodology adopted herein. Second, the shape of the first peak changed with seed size: with the seed fraction of 250−300 μm, the normalized population density at small size is high, contributing much to the overall population. With the seed fractions of 212−250 μm and 150−180 μm, the normalized population density drops off towards small size, indicating a diminishing contribution from particles of small size to overall population. This was in agreement with reports that larger crystals cause more secondary nucleation than smaller ones and that crystals are not capable of giving rise to fresh nuclei until they reach a critical size.[7] Using still finer seeds than those in the fraction of 150−180 μm may help to reduce secondary nucleation further. On the other hand, lengthened batch time as revealed by Figure 2a may aggravate attrition and lead to counter effects. A more effective approach is to increase seed loading so that the target size can be reduced and the batch time can be shortened.

2. Effects of Seed Loading. Two more experiments were conducted to mitigate the problem of secondary nucleation (runs 4 and 5 in Table 1). In run 4, the seed fraction of 212−250 μm was used, and the seed mass was doubled to 5.02 g ($M_S/M_P = 0.1079$). According to eq 3, the expected product size became 476 μm. In run 5, the seed fraction of 150−180 μm was used with a mass of 1.66 g ($M_S/M_P = 0.03846$), and the expected product size was also 476 μm. The resulting trajectories for accumulated mass of anti-solvent and PSD are given in Figure 3.

As expected, batch time was shortened by increasing seed loading as shown in Figure 3a. When seed fraction of 150−180 μm was used, the batch time was cut by 20 min. The improvement in PSD can be observed by comparing Figure 3b and Figure 2b. With a seed fraction of 212−250 μm, the peak in small size was flattened remarkably (CV equal to 23.67%) when seed loading was doubled. The average size of products was 514 μm, rather close to the expected product size of 476 μm. A similar improvement was obtained in the case of seed fraction 150−180 μm, with average size equal to 496 μm and *CV* equal to 25.89% respectively. All these changes mirror a successful suppression of secondary nucleation. Thereby seed loading turns out to be a useful parameter for tuning and refining the PSD of final product crystals.

3. Effects of PSD of Seeds. The previous experiments had used seeds in a narrow range to obtain narrow PSD of final products. However, it may be troublesome or time-consuming to sieve the crystals into such close fractions in industrial practice. It may be more convenient to simply use the undersize fraction from an existing screening unit in the production, or even the raw crystals from previous batches as seeds. In a further experiment (run 6 in Table 1), the fine fraction smaller than 125 μm (with an average size of 88 μm) was used. The PSD of seeds smaller than 125 μm was obtained by manually counting and measuring the second-largest dimension under the microscope since it is difficult to generate a reliable PSD by sieving for fines.

The target average size of product, $\bar{L}_P$,was again set at 476 μm for this run so that results could be compared with those in Figure 3. The mass of seeds smaller than 125 μm was 0.26 g ($M_S/M_P = 6.226 \times 10^{-3}$) from eq 3. The trajectories of anti-solvent mass and the PSD of seeds and products are shown in Figure 4a and b, respectively.

It can be seen in Figure 4a as well as Figures 2a and 3a that the resultant controlled anti-solvent addition profiles

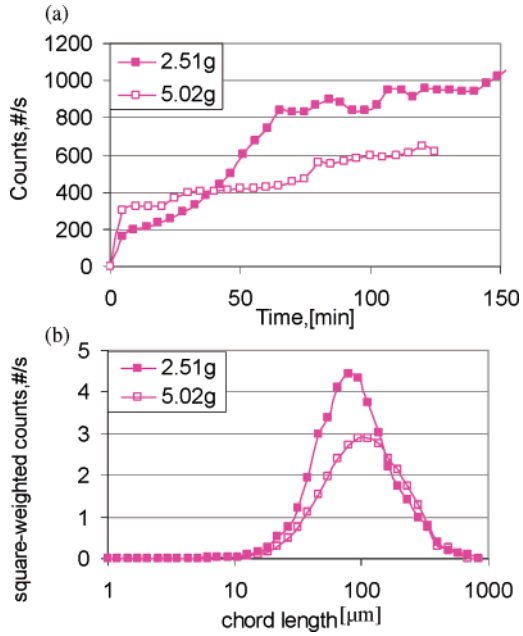

Figure 5. **FBRM data with two seed loadings. (a) Evolvement of counts of chord lengths with time, (b) chord length distribution at the end of operation.**

follow the common industrial expectation of a "cubic law".[25,26] The cubic profiles are confirmed by curve-fitting, as shown in Table 1.

A surprising observation in Figure 4b is the contrast in PSDs between seeds and products. With the one-sided parabolic distribution of seed particles, a unimodal PSD of products was still attained, although skewed to some degree when compared, for example, with that in Figure 3b. One possible explanation is that the growth of larger crystals is thwarted more by attrition and breakage than that of smaller ones,[3] so that there may be a maximum crystal size depending on the vessel configuration and agitator speed. The fact that smaller particles have more tendency to agglomerate than larger ones also contributes to the transformation of PSD from one-sided parabolic to unimodal.

4. Supporting Online Information from FBRM. As an online sensing device for the solid-side of crystallization processes, FBRM offers useful information for process monitoring and control. Take the two runs using seed fraction 212−250 μm as examples. The seed loadings were 2.51 g and 5.02 g, respectively (runs 2 and 4 in Table 1). Figure 5a shows changing counts of chord lengths with time, and Figure 5b shows the square-weighted CLDs of the slurry at the end of each run.

In Figure 5a it can be observed that after seeds were applied to the solution at the beginning of each run, the counts of chord lengths jumped from zero to a value in accordance with seed loadings. From then on the counts kept on increasing as crystallization proceeded. Obviously, two curves of counts followed different paths: the one with seed mass of 2.51 g increased more significantly than the other with seed mass of 5.02 g, reflecting the difference in the extent of secondary nucleation.

CLD data measured by FBRM provide an approximate correlation to the PSD in slurry. As shown in Figure 5b, the CLD obtained with seed mass of 5.02 g shifted towards large size with respect to that obtained with seed mass of 2.51 g. The square-weighted mean chord lengths were 141 and 122 μm, corresponding to the results of sieve analysis, 514 and 431 μm, respectively.

Conclusion

The effects of seeding at constant supersaturation were investigated in anti-solvent crystallization of paracetamol from a water−acetone mixture. Seed mass-size couples calculated from eq 3 are good starting points for deciding on a seeding strategy. After analysis of preliminary results, seed loading can be used to effectively tune and refine the PSD of the final product. Our results indicate that the ratio of target product size to initial seed size should not be too high to avoid excessive secondary nucleation. Under constant supersaturation, different seed mass-size couples led to similar PSD of the final products when the target product size was properly selected. Unimodal PSD can also be attained from undersized seeds, which may have practical implication for industrial operation. The applicability of the findings from this study to larger scale is currently being investigated.

Acknowledgment

We appreciate greatly the help from Professor Richard Braatz and his team from University of Illinois and Urbana-Champaign. The calibration data of ATR-FTIR in this study were processed using their chemometric software.

Nomenclature

c^* = equilibrium concentration of solute [g/g]
CV = coefficient of variation of particle size distribution [-]
t = any time during the process [min]
G_{met} = maximum allowable growth rate within metastable zone [m s^{-1}]
$\bar{L}$ = number-average size [μm]
M = mass [g]
T = temperature [°C]
$\dot{T}$ = cooling rate [°C s^{-1}]
ΔT_{met} = the maximum allowable undercooling [°C]
R^2 = determination coefficient in curve-fitting [-]
φ_v,φ_s = volume and surface shape factors of crystals [-]
ρ = crystal density [kg m^{-3}]
τ = the overall batch time [s]

Subscripts

sol = solvent
S, P = seed and product respectively
I, F = initial and final condition respectively

(25) Kim, S.; Lotz, B.; Lindrud, M.; Girard, K.; Moore, T.; Nagarajan, K.; Alvarez, M.; Lee, T.; Nikfar, F.; Davidovich, M.; Srivastava, S.; Kiang, S. Control of the Particle Properties of a Drug Substance by Crystallization Engineering and the Effect on Drug Product Formulation. *Org. Process Res. Dev.* **2005**, *9*, 894−901.
(26) Myerson, A. S. *Handbook of Industrial Crystallization*, 2nd ed.; Butterworth-Heinemann: Boston, 2002; p 245

Received for review March 13, 2006.
OP060058J